chemistry

MDPI

Article

Influence of the Support Composition on the Activity of Cobalt Catalysts Supported on Hydrotalcite-Derived Mg-Al Mixed Oxides in Ammonia Synthesis

Magdalena Zybert [1], Hubert Ronduda [1,*], Aleksandra Dziewulska [1], Kamil Sobczak [2], Andrzej Ostrowski [1], Wojciech Patkowski [1] and Wioletta Raróg-Pilecka [1]

[1] Faculty of Chemistry, Warsaw University of Technology, Noakowskiego 3, 00-664 Warsaw, Poland; magdalena.zybert@pw.edu.pl (M.Z.); aleksandra.dziewulska.stud@pw.edu.pl (A.D.); aostrowski@ch.pw.edu.pl (A.O.); wpatkowski@ch.pw.edu.pl (W.P.); wiola@ch.pw.edu.pl (W.R.-P.)
[2] Biological and Chemical Research Centre, University of Warsaw, Żwirki i Wigury 101, 02-089 Warsaw, Poland; ksobczak@cnbc.uw.edu.pl
* Correspondence: hubert.ronduda.dokt@pw.edu.pl

Abstract: Recently, catalysts with hydrotalcites and hydrotalcite-derived compounds have attracted particular interest due to their specific properties, mostly well-developed texture, high thermal stability, and favorable acid–base properties. In this work, we report the investigation of ammonia synthesis on barium-promoted cobalt catalysts supported on hydrotalcite-derived Mg-Al mixed oxides with different Mg/Al molar ratios. The obtained catalysts were characterized using TGA-MS, nitrogen physisorption, XRPD, TEM, STEM-EDX, H_2-TPD, CO_2-TPD, and tested in ammonia synthesis (470 °C, 6.3 MPa, H_2/N_2 = 3). The studies revealed that the prepared Mg-Al mixed oxides are good candidates as support materials for Co-based catalysts. However, interestingly, the support composition does not influence the activity of Ba/Co/Mg-Al catalysts. The change in Mg/Al molar ratio in the range of 2–5 did not significantly change the catalyst properties. All the catalysts are characterized by similar textural, structural, and chemisorption properties. The similar density of basic sites on the surface of the studied catalysts was reflected in their comparable performance in ammonia synthesis.

Keywords: hydrotalcite; mixed oxides; supported catalyst; cobalt catalyst; ammonia synthesis

Citation: Zybert, M.; Ronduda, H.; Dziewulska, A.; Sobczak, K.; Ostrowski, A.; Patkowski, W.; Raróg-Pilecka, W. Influence of the Support Composition on the Activity of Cobalt Catalysts Supported on Hydrotalcite-Derived Mg-Al Mixed Oxides in Ammonia Synthesis. *Chemistry* **2022**, *4*, 480–493. https://doi.org/10.3390/chemistry4020035

Academic Editors: Detlef W. Bahnemann and Guoqi Zhang

Received: 3 April 2022
Accepted: 16 May 2022
Published: 17 May 2022

1. Introduction

Ammonia synthesis is an important chemical process upon which many industries are based, including the production of fertilizers or explosives. The estimated global production of ammonia is approximately 150 million metric tons and is projected to increase by 2.3% per year [1–3]. Although the Haber–Bosch process has been carried out for over 100 years, the continuously increasing demand for ammonia forces the need to search for new technological solutions to reduce energy consumption and increase the entire process' efficiency [4,5]. Two types of catalytic systems which have been used in the industry for a long time are a promoted iron catalyst and a carbon-supported ruthenium catalyst. Despite the fact that the former exhibits a long working time and low cost, it does not provide a high reaction rate at a high ammonia concentration. On the other hand, due to the high cost of ruthenium, the latter is used only in a few industrial plants. In recent years, attempts have been made to deposit ruthenium onto other supports, e.g., MgO-CeO_2 [6,7], MgO [8], $BaCeO_3$ [9], $BaZrO_3$ [10], ZrO_2 [11], and rare-earth oxides [12–17]. Despite the high activity of such systems, the high price of ruthenium and poor stability of Ru nanoparticles due to sintering effectively discourages their use on a large scale. Therefore, the current research on ammonia synthesis is focused on searching for new catalysts with a favorable activity-to-price ratio, i.e., characterized by higher activity than the iron catalyst and a lower price than the ruthenium catalyst.

Although cobalt is not highly active in the synthesis of ammonia, studies by Hagen et al. [18,19] have shown that the addition of barium significantly increases the catalytic activity of this metal. This was a significant impetus for searching for an alternative catalytic system for ammonia synthesis with cobalt as the active phase. Among the active catalytic systems found in the literature are unsupported cobalt catalysts promoted with barium [20–22] or rare earth metals (especially cerium [20,21,23] and lanthanum [24]). However, the application of supports allows for better use of the catalyst potential during the technological process by reducing the cost of catalyst production, increasing the active phase dispersion, and the size and morphology of its particles. So far, literature reports describe the use of only a few supports for cobalt, mainly activated carbons [25,26], cerium oxide [27–29] and recently magnesium oxide [30] or mixed MgO-Ln_2O_3 oxides (Ln = La, Nd, Eu) [31–35]. A more sophisticated novel type of support such as electrides (e.g., C12A7:e^-) with excellent promotion effect due to their strong electron-donating ability [2,36,37] or hydride support materials (e.g., LiH, BaH_2) changing the reaction pathway (a two-active-center mechanism) [38,39] are also reported. Rare-earth metal nitrides such as CeN were reported recently as very effective support promoting ammonia synthesis over a Co-based catalyst [40]. However, all these systems were tested only under mild conditions (i.e., ambient pressure, low temperature), applicable only to small-scale green ammonia production via the Haber–Bosch process.

A very interesting type of support investigated as an alternative to the standard support systems are hydrotalcites, also known as layered double hydroxides, with the general formula $\left[M^{II}_{1-x}M^{III}_{x}(OH)_2\right]^{x+}\left[A^{n-}\right]_{x/n}\cdot mH_2O$, where x—mole fraction of a trivalent metal, n—valence of an interlayer anion, and m—number of water molecules [41–44]. These materials exhibit basic properties depending on the amount of metal introduced into the brucite layer. The number and strength of acid and basic sites are influenced by the nature and amount of the trivalent cation (M^{II}/M^{III} ratio) [45]. This is of great importance in the implementation of hydrotalcite materials as supports or support precursors in the preparation of catalysts. The acid–base properties of supports play a crucial role in the formation of active centers, the nature of which results in the activity of the catalytic system [46]. In the synthesis of ammonia, the catalysts should be characterized by a large number of medium and strong basic centers, which can be achieved by using more basic supports. These centers are particularly desirable due to the rate-determining step, i.e., dissociation of the nitrogen molecule. This process can be accelerated by donating electrons from the surface of the support to d-orbitals of metal atoms (the active phase) and further to the anti-binding orbitals of nitrogen molecules adsorbed on the surface of this metal. In order to be an efficient electron donor, a support needs the presence of Lewis basic centers, which are identified with medium and strong basic sites represented by, e.g., oxide anions. Such basic systems are easy to obtain with the use of hydrotalcites-like materials. An additional advantage of mixed oxides obtained from the thermal decomposition of hydrotalcites in temperatures below 500 °C is a developed texture, i.e., greater porosity and specific surface area than that of the untreated hydrotalcite [42]. Moreover, hydrotalcite-derived oxides exhibit high thermal resistance, which is an excellent advantage in high-temperature processes. In catalysts containing transition metals, such as ruthenium supported on hydrotalcite-derived materials, a high degree of metal phase dispersion is observed [47]. Due to these properties, catalysts using hydrotalcites and hydrotalcite-derived compounds have recently attracted particular interest as redox and acid–base catalysts. Hydrotalcite-derived mixed-oxides have already been studied as supports for ruthenium in ammonia synthesis catalysts. It was reported that Ru supported on Mg-Al mixed oxide is an efficient catalyst of activity higher than that of Ru supported on conventional supports such as MgO or Al_2O_3 [46,47].

In this study, a series of barium-promoted cobalt catalysts supported on hydrotalcite-derived Mg-Al mixed oxides with a variable Mg/Al molar ratio was prepared and characterized to understand the relationship between the support composition and catalyst properties. The obtained materials were characterized using TGA-MS, nitrogen physisorption, XRPD, TEM, STEM-EDX, H_2-TPD, CO_2-TPD. The influence of Mg/Al molar ratio on

the physicochemical characteristics and performance of the catalysts in ammonia synthesis reaction was the object of detailed analysis.

2. Materials and Methods

2.1. Preparation of Mg-Al Mixed Oxides

A series of Mg-Al hydrotalcites with various Mg/Al molar ratios (2, 3, 4, and 5) was synthesized by co-precipitation. In a typical procedure, an aqueous solution A was prepared by dissolving the proper amounts of $Mg(NO_3)\cdot 6H_2O$ (Chempur, Karlsruhe, Germany, pure p.a.) and $Al(NO_3)_3\cdot 9H_2O$ (Chempur, Karlsruhe, Germany, pure p.a.) in distilled water, and an alkaline solution B was prepared by mixing of NaOH (Chempur, Karlsruhe, Germany, pure p.a.) and Na_2CO_3 (Chempur, Karlsruhe, Germany, p.a.) aqueous solutions with a molar ratio of 10:1. Both solutions A and B were simultaneously added dropwise into a beaker containing 750 mL of distilled water at 30 °C under vigorous stirring. During the precipitation, the pH value was maintained at 10 by controlling the dropping rate of solution B. The formed suspension was aged at 80 °C for 18 h under stirring. The precipitate was filtered, followed by washing with distilled water. After drying, the resulting powder was calcined at 500 °C for 4 h to obtain Mg-Al mixed oxides.

2.2. Preparation of Ba/Co/Mg-Al Catalysts

A series of Ba/Co/Mg-Al catalyst precursors were synthesized by wet impregnation. The Co content was fixed at 40 wt %. In a typical procedure, the proper amount of $Co(NO_3)\cdot 6H_2O$ (Acros Organics, Waltham, MA, USA, 98+%) was dissolved in distilled water, followed by the addition of Mg-Al mixed oxide. After impregnation, the water was removed using a rotatory evaporator, maintaining the bath temperature at 60 °C. The resulting solid was dried at 120 °C for 18 h and calcined at 500 °C for 4 h. Ba was introduced in the form of $Ba(NO_3)_2$ using the same procedure as described above, but without the calcination process. The amount of Ba was fixed at 3 wt %. Before testing, each catalyst precursor was reduced at 550 °C to form an active catalyst Ba/Co/Mg-Al. The benchmark unpromoted cobalt catalyst supported on 5Mg-Al mixed oxide (Co/5Mg-Al) was also prepared using the procedure described above.

2.3. Characterization Methods

Thermogravimetric analysis of Mg-Al hydrotalcites was carried out in a thermogravimetric analyzer (NETZSCH STA449C) integrated with a quadrupole mass spectrometer (NETZSCH QMS Aëolos 403C). A sample of mass of 30 mg was loaded onto an alumina plate and heated up to 1000 °C at a ramping rate of 10 °C min^{-1} under airflow of 100 cm^3 min^{-1}. The signals of m/e = 18 and 44 were registered for H_2O and CO_2, respectively.

The surface area and total pore volume of the support precursors (hydrotalcites) and supports (mixed oxides) were determined from N_2 physisorption adsorption/desorption isotherms at liquid nitrogen temperature (−196 °C) using an ASAP 2020 analyzer (Micromeritics, Caringbah, Australia). Before the measurement, 300 mg of a sample was degassed under vacuum at 50 °C for 1 h and next at 80 °C for 4 h. The surface area and pore volume were determined by fitting the experimental data to the BET and BJH adsorption isotherm models. N_2 adsorption/desorption isotherms were also collected for the catalysts. To this end, each catalyst precursor was reduced at 550 °C for 10 h under H_2 flow (40 cm^3 min^{-1}). Then the sample was degassed at 200 °C for 2 h, and the experiment was conducted.

Powder X-ray diffraction patterns were recorded on a Bruker D8 Advance diffractometer equipped with an LYNXEYE position-sensitive detector, using Cu-Kα radiation (λ = 0.15418 nm). The data were collected in the Bragg–Brentano (θ/θ) horizontal geometry between 10° and 70° (2θ) in a continuous scan using 0.03° steps 10 s/step. The diffractometer incident beam path was equipped with a 2.5° Soller slit and a 1.14° fixed divergence slit, while the diffracted beam path was equipped with a programmable anti-scatter slit

(fixed at 2.20°), a Ni β-filter, and a 2.5° Soller slit. Data were collected under standard laboratory conditions.

Transmission electron microscope (TEM) measurements were carried out on a FEI Talos F200X microscope operated at 200 kV. Observations were performed in TEM and scanning transmission electron microscopy (STEM) mode using high-angle annular dark-field (HAADF) imaging. Energy dispersive X-ray spectroscopy (EDX) using a Super-X system with four silicon drift detectors (SDDs) was applied to detect differences in local chemical composition.

H_2 temperature-programmed desorption was carried out in an AutoChem II 2920 analyzer (Micromeritics) equipped with a thermal conductivity detector (TCD). Before a measurement, 500 mg of a catalyst precursor was reduced at 550 °C for 18 h under H_2 (40 cm^3 min^{-1}) and then purged at 570 °C for 2 h under Ar flow (40 cm^3 min^{-1}). After cooling to 150 °C, H_2 flow was introduced (40 cm^3 min^{-1}) for 15 min. Then the sample was cooled to 0 °C and kept at that temperature for another 15 min. Subsequently, the sample was purged with Ar at 0 °C until the baseline was stable. The experiment was conducted in Ar flow (40 cm^3 min^{-1}) at a heating rate of 5 °C min^{-1} up to 700 °C.

CO_2 temperature-programmed desorption was carried out using the same AutoChem II 2920 analyzer (Micromeritics) equipped with a thermal conductivity detector (TCD). Before a measurement, 500 mg of a catalyst precursor was reduced at 550 °C for 18 h under H_2 (40 cm^3 min^{-1}) and then purged at 570 °C for 2 h under He flow (40 cm^3 min^{-1}). After cooling to 40 °C, pure CO_2 was introduced at a flow of 40 cm^3 min^{-1} for 2 h. Subsequently, the sample was purged with flowing He at 40 °C until the baseline was stable. The experiment was conducted in flowing He (40 cm^3 min^{-1}) at a heating rate of 5 °C min^{-1} up to 700 °C.

Catalytic activity measurements in ammonia synthesis were performed in a tubular flow reactor, as described previously [32]. Before testing, 500 mg of a catalyst precursor was activated in the reaction mixture at a flow rate of 30 dm^3 h^{-1} (H_2/N_2 = 3, purity 99.99995 vol%) at atmospheric pressure at different temperatures, i.e., 470 °C (72 h) → 520 °C (24 h) → 550 °C (48 h). Under steady-state conditions of temperature (470 °C), pressure (6.3 MPa), and gas flow rate (70 dm^3 h^{-1}), the ammonia concentration in the outlet gas was measured interferometrically, and then the NH_3 synthesis rate was determined. The uncertainty in the NH_3 production rate was ±1%. The detailed calculation equations can be found in our previous work [32].

3. Results and Discussion

3.1. Physicochemical Characteristics of Mg-Al Hydrotalcite and Mg-Al Mixed Oxides

Thermal decomposition of the obtained Mg-Al hydrotalcites with a variable Mg/Al molar ratio was investigated using thermogravimetric analysis. Regardless of chemical composition, all of the obtained materials are characterized by a similar course of thermal decomposition, typical for hydrotalcite materials described in the literature [41,48,49]. Figure 1 shows an exemplary TGA-MS curve of the 5Mg-Al support precursor (hydrotalcite) of Mg/Al molar ratio equal to 5. The decomposition process is clearly divided into two noticeable steps. The first mass loss (about 13%) was recorded at a temperature up to 250 °C and accompanied by a mass signal of m/e = 18 corresponding to dehydration, i.e., removal of physisorbed water and interlayer structural water. A small peak was also visible on the mass signal of m/e = 44 assigned to the release of physically bound CO_2. The second mass loss (about 28%) in the temperature range of 250–550 °C takes place due to dehydroxylation of brucite layers confirmed by the peak on the m/e = 18 mass signal. Moreover, a distinct peak corresponding to carbon dioxide evolution (m/e = 44) indicates decarboxylation, i.e., removal of carbonate anions from the interlayer spaces. The release of the gaseous compounds generates a substantial porosity in the calcined hydrotalcite-derived mixed oxides and a significant increase in the surface area of these materials [42]. This is confirmed by the results of textural studies. A representative N_2 adsorption–desorption curve for the support precursor of Mg/Al molar ratio equal to 5, illustrating the nature of the isotherms

recorded for all the tested materials, is shown in Figure 2. According to the IUPAC classification, the samples exhibited the type IV adsorption isotherm [50], characteristic of mesoporous solid materials with H3 type hysteresis loop, indicating the presence of pores formed from non-parallel planes, i.e., slit-shaped pores. After the thermal treatment of the support precursors (hydrotalcites), the type of the N_2 adsorption–desorption isotherms remained unchanged for the supports (mixed oxides). However, the amount of adsorbed nitrogen increased, indicating the development of a porous system of the Mg-Al mixed oxides due to CO_2 evolution during decomposition of the interlayer CO_3^{2-} anions. No clear correlation was observed between the composition, i.e., Mg/Al molar ratio of the support precursors and their textural parameters. For all the obtained hydrotalcites, the surface area was in the range of 80–118 $m^2\ g^{-1}$. They were also characterized by a similar pore volume in the range of 0.5–0.7 $cm^3\ g^{-1}$ (Table 1). Thermal decomposition of hydrotalcites leads to fine crystalline mixed metal oxides. It is manifested in a visible increase in the value of textural parameters for mixed oxides—the surface area is 2–3 times higher, and the pore volume is almost twice larger compared to the untreated hydrotalcites. Analyzing the obtained results makes it possible to indicate some structure-forming effect of Al_2O_3 oxide. The surface area decreased with increasing Mg/Al molar ratio (i.e., when Al_2O_3 content decreased). These results are in agreement with the report of Jinesh et al. [51], indicating the same effect for the materials of Mg/Al molar ratio from 1 to 5. Nevertheless, there is an ambiguous viewpoint in the literature regarding the influence of Mg/Al molar ratio on the textural parameters of the obtained mixed oxides [52,53].

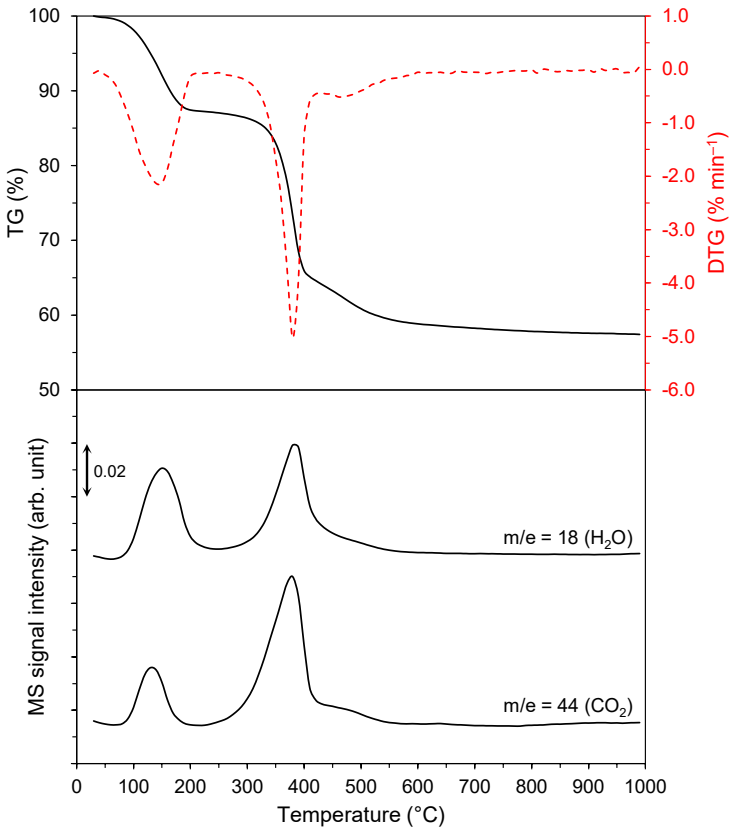

Figure 1. TGA-MS curve of the 5Mg-Al hydrotalcite (heating in airflow, temperature range 30–1000 °C); (**top**) TG and DTG curves, (**bottom**) selected mass signals of H_2O and CO_2 (m/e = 18 and 44).

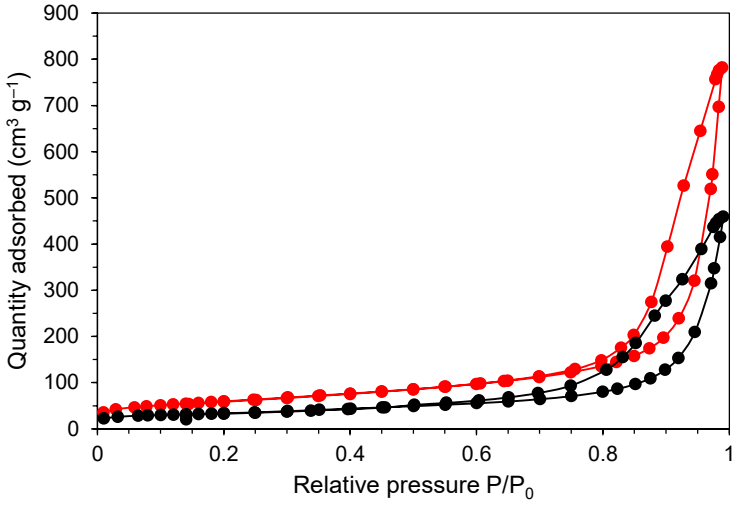

Figure 2. Nitrogen adsorption–desorption isotherms for the 5Mg-Al hydrotalcite (black lines) and 5Mg-Al mixed oxide (red lines).

Table 1. Physicochemical properties of the support precursors (hydrotalcites) and the supports (mixed oxides).

Support	Mg/Al Molar Ratio [1]	Support Precursor (Hydrotalcite)		Support (Mixed Oxide)	
		Surface Area [2] (m^2 g^{-1})	Pore Volume [3] (cm^3 g^{-1})	Surface Area [2] (m^2 g^{-1})	Pore Volume [3] (cm^3 g^{-1})
2Mg-Al	1.8	84	0.6	239	1.0
3Mg-Al	2.9	101	0.6	235	1.0
4Mg-Al	3.9	81	0.5	212	0.9
5Mg-Al	4.8	118	0.7	210	1.2

[1] Mg/Al molar ratio determined by inductively coupled plasma optical emission spectroscopy (ICP-OES). [2] Surface area estimated based on the Brunauer–Emmett–Teller (BET) method. [3] Pore volume estimated based on the Barret–Joyner–Halenda (BJH) method.

The structural properties of the support materials both before and after thermal treatment were determined using X-ray powder diffraction (XRPD). Figure 3a depicts the diffraction patterns of all the support precursors with various Mg/Al molar ratio, typical of a layered double hydroxide structure [54]. For the 2Mg-Al support precursor, the clear, sharp, and symmetric diffraction lines indicate a well-crystallized, highly ordered hexagonal structure with the space group R-3m. Along with the increase in Mg content, the reflections are less intense and much broader, which indicates a decrease in the degree of crystallinity of the materials. This was reflected in the determined crystallite size decreasing from 14 nm to 8 nm with increasing Mg/Al molar ratio from 2 to 5 (Table 2). The hydrotalcite lattice structural parameters calculated from the obtained data (Table 2) clearly show that introducing a higher amount of Mg^{2+} ions leads to some modification of the structure of the hydrotalcite materials. The values of parameters *a* and *c* increased with increasing Mg/Al molar ratio. It is in accordance with the literature reports [42] indicating that the value of parameter *a*, related to metal–metal distance in the brucite-like layer, increases when more Al^{3+} ions (0.53 Å) in these layers are substituted by Mg^{2+} ions, whose ionic radius is larger (0.65 Å). It also influences the interlayer spacing, which leads to an increase in parameter *c*.

Thermal treatment of the support precursors (hydrotalcites) led to their decomposition and change of the phase composition of the materials into mixed oxides. The diffraction patterns (Figure 3b) for all the samples showed reflections at 2θ angles around 43° and 63° consistent with the presence of the MgO periclase phase (PDF#45-0946). The lack of reflections of Al-containing phases indicates that they may be present in a highly dispersed form. Any other crystalline phases containing Mg or Al were not detected. Only a few

weak signals at low values of 2θ angles (10–35°) were observed. They may be attributed to a small amount of the hydrotalcite phase, which did not completely decompose.

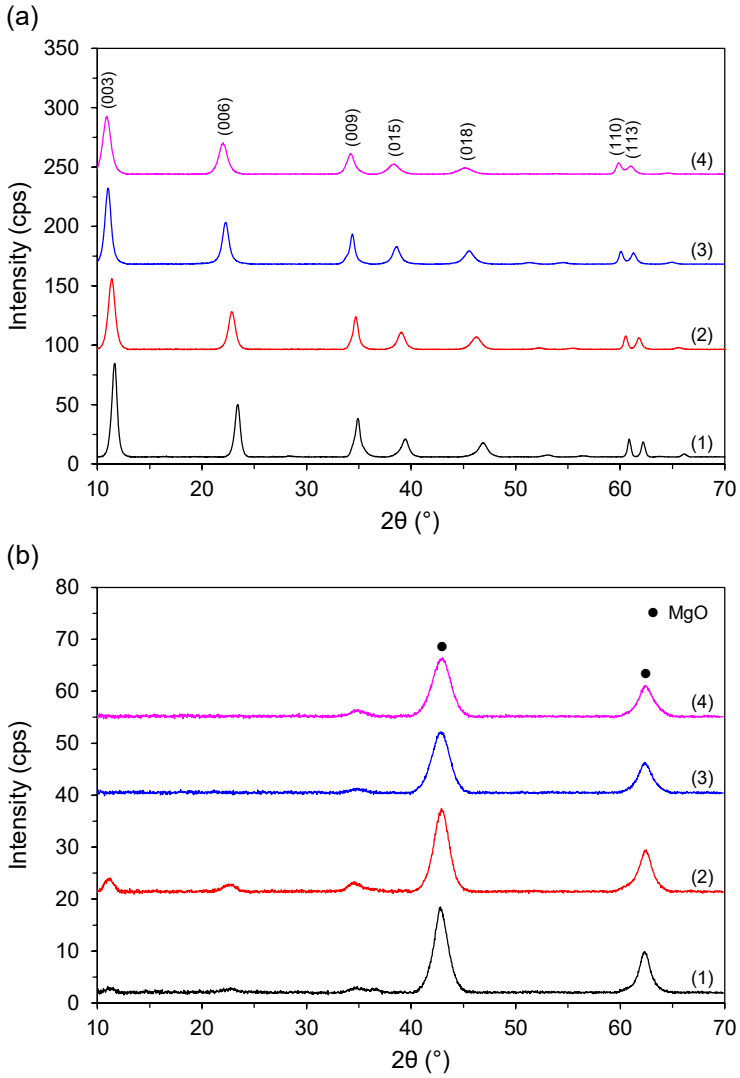

Figure 3. XRPD patterns of the (**a**) hydrotalcites (the reflections typical of a layered double hydroxide structure are marked) and (**b**) mixed oxides with various Mg/Al molar ratio: (1) 2Mg-Al, (2) 3Mg-Al, (3) 4Mg-Al, (4) 5Mg-Al.

Table 2. Rietveld refinement structural data of the support precursors (hydrotalcites).

Support Precursor (Hydrotalcite)	*a* (Å)	*c* (Å)	V (Å^3)	Crystallite Size (nm)
2Mg-Al	3.047	22.83	183.5	14
3Mg-Al	3.063	23.40	190.1	11
4Mg-Al	3.075	23.83	195.2	12
5Mg-Al	3.087	24.18	199.6	8

The detailed structural studies using transmission electron microscopy (TEM) and high-angle annular dark-field scanning transmission electron microscopy (STEM-HAADF) were performed for the selected support (5Mg-Al) to characterise its microstructure and morphology. As shown in Figure 4a,b, the support comprises two crystalline phases: MgO and Al_2O_3. The magnesium oxide phase occurs in a rod-like structure clearly visible in Figure 4b. The aluminium oxide phase occurs as small crystallites of a few or several

nanometres that form a support matrix, porous in some places. The EDX mapping confirms a uniform distribution of Al in the support (Figure 4d,h) and the concentration of Mg on the rod-like particles (Figure 4e,g).

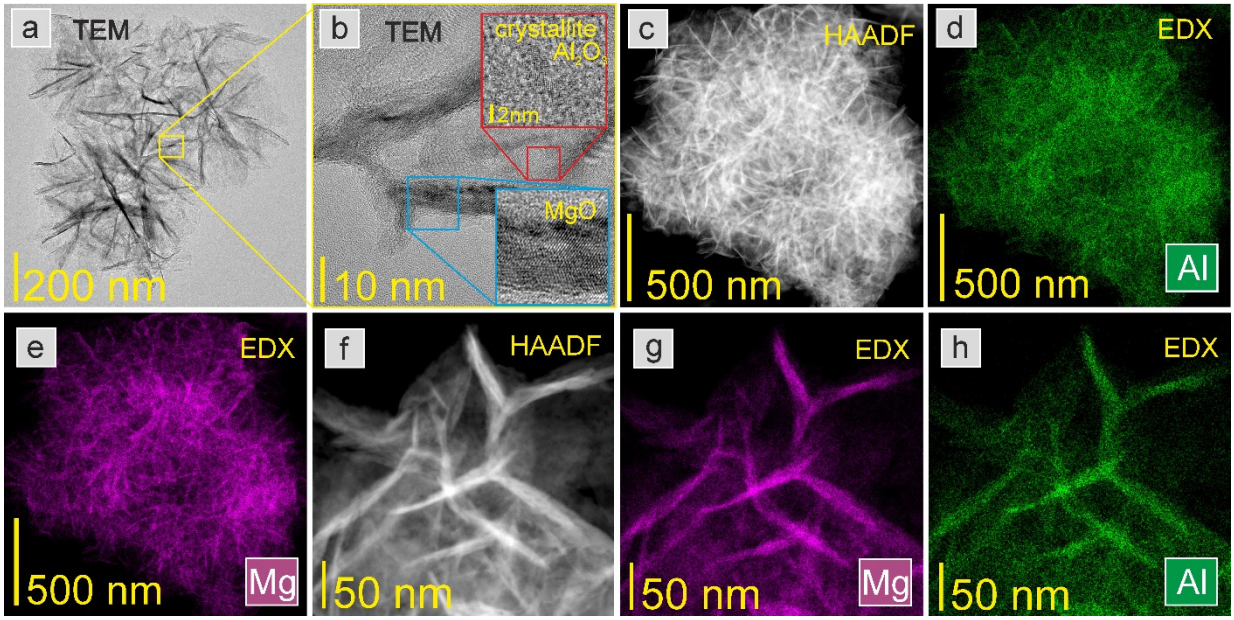

Figure 4. (**a**) TEM image of the 5Mg-Al support with (**b**) an enlarged fragment showing the polycrystalline structure of the compounds (MgO and Al_2O_3). The crystallite Al_2O_3 and the nanorod-like MgO nanostructure were presented in the inset. (**c**) STEM-HAADF image and EDX mapping presenting a uniform distribution of the elements: (**d**) aluminium and (**e**) magnesium. (**f**) STEM-HAADF image of the enlarged fragment of the 5Mg-Al support and corresponding EDX investigation of the distribution of elements: (**g**) magnesium and (**h**) aluminium.

3.2. Characteristics of the Ba/Co/Mg-Al Catalysts

The results of the surface area measurements for the barium-promoted cobalt catalysts supported on Mg-Al mixed oxides are summarised in Table 3. For the studied catalysts, no correlation was observed between the support composition, i.e., Mg/Al molar ratio, and the surface area of the catalysts, which is in the range of 125–146 $m^2\ g^{-1}$. However, it should be noted that the surface area for the catalysts is about 40% lower in comparison to the surface area of the supports (Table 1). This is due to successive deposition of the active phase precursor (cobalt salt) and then the promoter precursor (barium salt), which occupies part of the surface and crystallizes in the pores of the support.

Table 3. Physicochemical properties and catalytic activity in the ammonia synthesis reaction of the barium-promoted cobalt catalysts supported on Mg-Al mixed oxides.

Catalyst	Surface Area [1] ($m^2\ g^{-1}$)	Total Basicity [2] ($\mu mol\ g^{-1}$)	Density of Basic Sites [3] ($\mu mol\ m^{-2}$)	Cobalt Crystallite size [4] (nm)	Reaction Rate [5] ($g_{NH_3}\ g_{cat}^{-1}\ h^{-1}$)
Ba/Co/2Mg-Al	134	287	2.1	7.7	0.41
Ba/Co/3Mg-Al	146	266	1.8	6.9	0.42
Ba/Co/4Mg-Al	135	243	1.8	7.9	0.46
Ba/Co/5Mg-Al	125	236	1.9	7.9	0.50

[1] Surface area estimated based on the Brunauer–Emmett–Teller (BET) method for the reduced catalysts (after heating in hydrogen flow at 550 °C for 10 h). [2] Calculated based on the total amount of CO_2 desorbed from the catalyst surface, in relation to 1 g of the reduced catalyst. [3] Calculated based on the total amount of CO_2 desorbed from the catalyst surface and surface area for the reduced catalysts (after heating in hydrogen flow at 550 °C for 10 h). [4] Estimated based on XRPD results. [5] NH_3 synthesis reaction conditions: 470 °C, 6.3 MPa, H_2/N_2 = 3.70 $dm^3\ h^{-1}$.

Figure 5 depicts the XRPD patterns of the Ba/Co/Mg-Al catalysts in the reduced form. All the patterns show the presence of reflections assigned to MgO periclase phase (PDF#45-1225) derived from the catalyst support. Moreover, reflections at 44.2° and 51.5° ascribed to face-centred cubic cobalt (PDF#15-0806) are visible. The cobalt crystallite size is shown in Table 3. Interestingly, Co crystallites have nearly the same sizes, ca. 7–8 nm, regardless of the Mg-Al molar ratio of the support on which cobalt was deposited. The lack of reflections attributed to Ba-containing phases indicates that barium promoter is present in the catalysts in the form undetectable by XRPD, i.e., amorphous or/and highly dispersed.

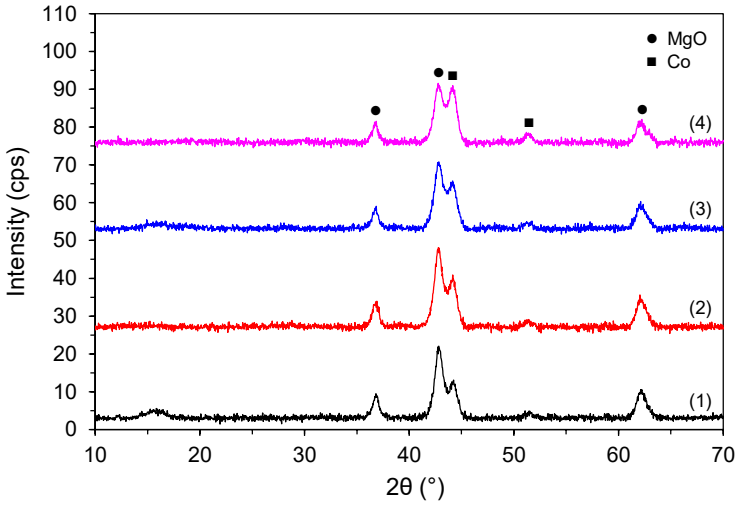

Figure 5. XRPD patterns of the Ba/Co/Mg-Al catalysts supported on hydrotalcite derived Mg-Al mixed oxides with various Mg/Al molar ratio: (1) 2Mg-Al, (2) 3Mg-Al, (3) 4Mg-Al, (4) 5Mg-Al.

The microstructure and morphology for the selected catalyst (Ba/Co/5Mg-Al) were studied using transmission electron microscopy (TEM) and high-angle annular dark-field scanning transmission electron microscopy (STEM-HAADF). Figure 6a–c show a uniform distribution of the crystalline cobalt nanoparticles on the 5Mg-Al support evidenced in the EDX map of cobalt (Figure 6d). The series of the EDX maps (Figure 6e–k) also confirms the homogeneous distribution of the other components on the catalyst surface. Based on the series of EDX maps, a histogram of the size of cobalt nanoparticles was prepared. The data fit to the LogNormal distribution. The estimated average cobalt nanoparticle size is 14.8 nm. This means that the active phase forms polycrystalline particles composed of smaller crystallites, which is consistent with the results of the XRPD analysis (Table 3).

The chemisorption ability of the studied catalysts was determined by temperature-programmed desorption of hydrogen. Figure 7 shows the H_2-TPD profiles for the Ba/Co/Mg-Al catalysts. Two distinct H_2 desorption peaks were recorded: the low-temperature peak with a high intensity and the maximum ca. 120 °C and a much smaller medium-temperature peak with the maximum at approximately 350 °C. They were attributed to the desorption of hydrogen atoms bound to the cobalt surface weakly and moderately, respectively. No high-temperature (>550 °C) peaks were detected. This indicates the lack of active sites which strongly bind hydrogen on the cobalt surface. It is favorable from the point of view of ammonia synthesis because on the studied catalyst surface there are no active sites that would be blocked by strongly bound hydrogen and thus not involved in the reaction. The increase in the Mg/Al molar ratio of the support slightly decreased the intensity of the desorption peaks and slightly shifted their positions to lower temperatures. This may suggest that the increase in the MgO content in the support has almost no significant influence on the adsorption strength of hydrogen on the cobalt surface.

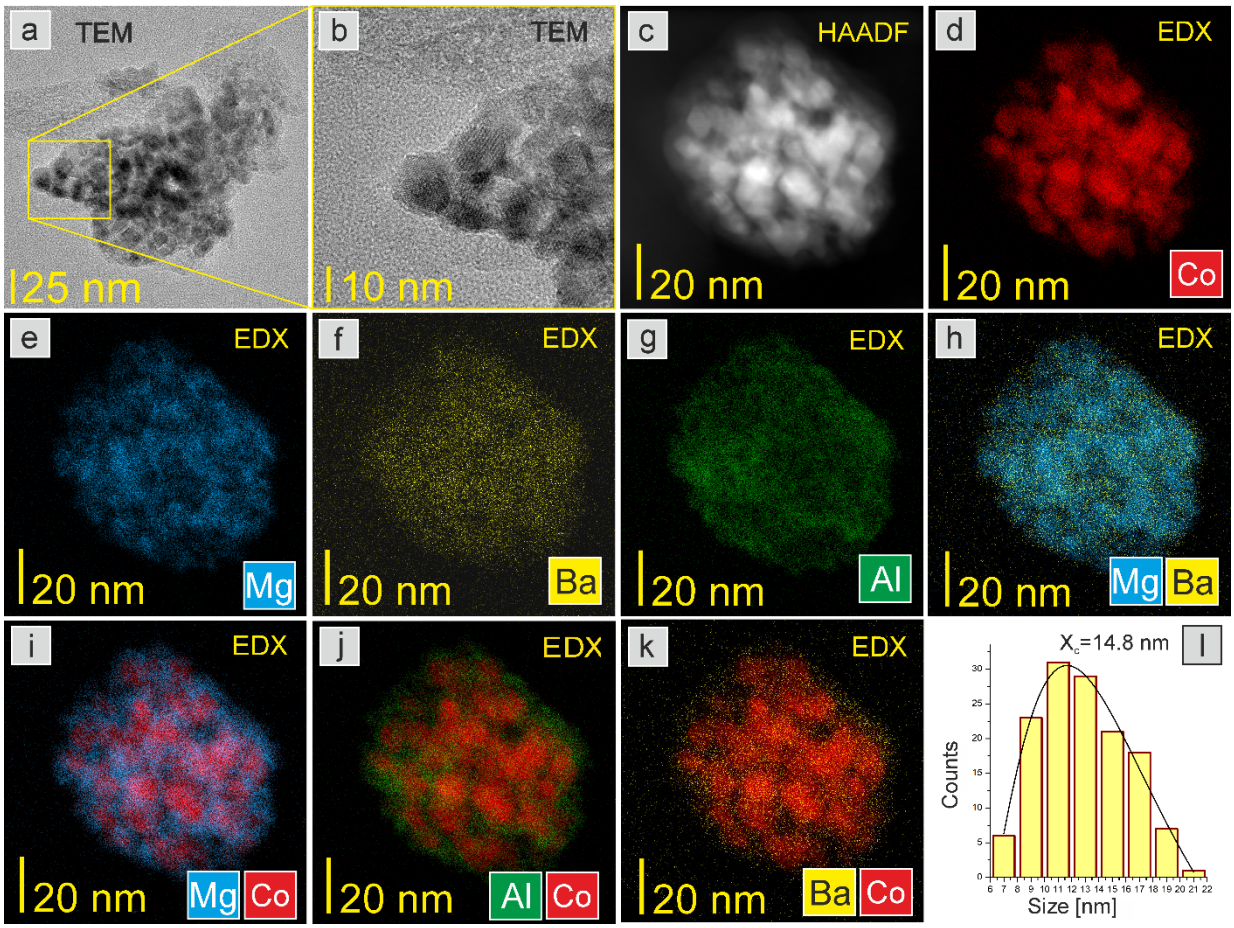

Figure 6. (**a**) TEM image of the Ba/Co/5Mg-Al catalyst with (**b**) an enlarged fragment showing the crystalline structure of the catalyst. (**c**) STEM-HAADF image and corresponding EDX mapping showing a uniform distribution of the elements: (**d**) cobalt, (**e**) magnesium, (**f**) barium, and (**g**) aluminium. Additionally, EDX maps with two elements are included: (**h**) Mg-Ba, (**i**) Mg-Co, (**j**) Al-Co, and (**k**) Ba-Co. (**l**) Histogram of the cobalt nanoparticles.

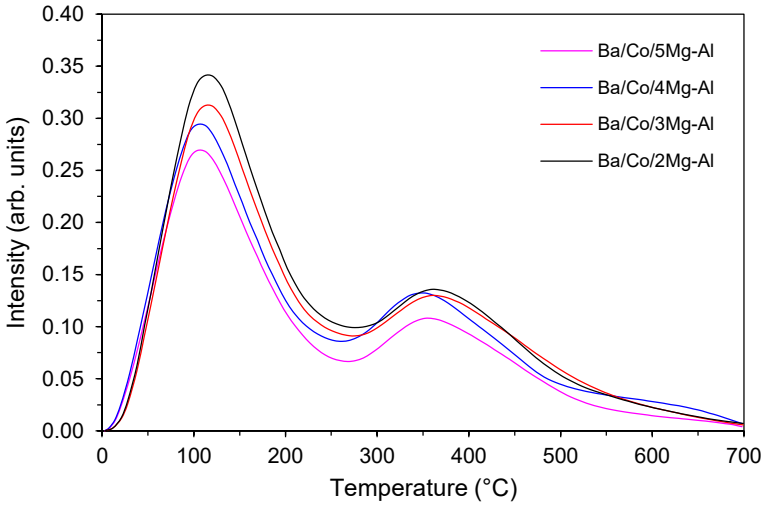

Figure 7. H_2-TPD profiles of the Ba/Co/Mg-Al catalysts supported on mixed oxides with various Mg/Al molar ratios.

Figure 8 shows the CO_2-TPD profiles of the Ba/Co/Mg-Al catalysts. The CO_2 desorption profiles recorded for all the catalysts consist of two peaks, i.e., the low-temperature peak (up to 250 °C) centred at ca. 150 °C and the broad medium-temperature peak (in the range of 250–600 °C) attributed to adsorption sites which bind CO_2 weakly and moderately, respectively. Nevertheless, only the latter is associated with Lewis basic sites, resulting from the presence of various lower coordinated oxygen species (e.g., O_2^{2-}, O^-). These sites are the most important from the point of view of the mechanism of ammonia synthesis. They enable the effective donation of electrons to the active metal (cobalt), facilitating N_2 dissociation (rate-determining step of ammonia synthesis reaction) by weakening the N≡N bond. Along with the increase in the Mg/Al molar ratio, a decrease in the intensity of the peaks and a gradual shift of the maximum of the medium-temperature peak towards higher temperatures (from 300 °C for Ba/Co/2Mg-Al to 350 °C for Ba/Co/5Mg-Al) was observed. This may indicate an increase in the binding strength of the probe molecule on the basic sites with increasing MgO content in the support. Table 3 lists the amounts of CO_2 desorbed from the Ba/Co/Mg-Al catalyst surface (obtained by the CO_2-TPD curve integration) related to the mass or the surface area of the reduced catalysts representing the total basicity or density of basic sites, respectively. For the studied catalysts, with the increase in the Mg/Al molar ratio, the total basicity decreased slightly (by a maximum of 17% when the Mg/Al molar ratio was changed from 2 to 5). However, considering the surface area of the reduced catalysts, it is visible that the density of basic sites for all the catalysts is similar and equals approximately 2 μmol m^{-2}. Similar observations concerning the decrease of the total basicity with increasing Mg/Al molar ratio were presented previously by Hájek et al. [45]. Moreover, Kuśtrowski et al. [55] reported that, in the case of materials after thermal treatment at temperatures higher than 450 °C, the amount of basic sites decreased compared to materials after treatment at lower temperatures. However, there is no consensus among researchers as to the unequivocal correlation between the surface basicity and the Mg/Al molar ratio. Some reports indicated the opposite results [52]. A critical analysis of the reported data shows that this relationship is more complex and is also influenced by other factors, including method of synthesis and conditions of thermal treatment of these materials.

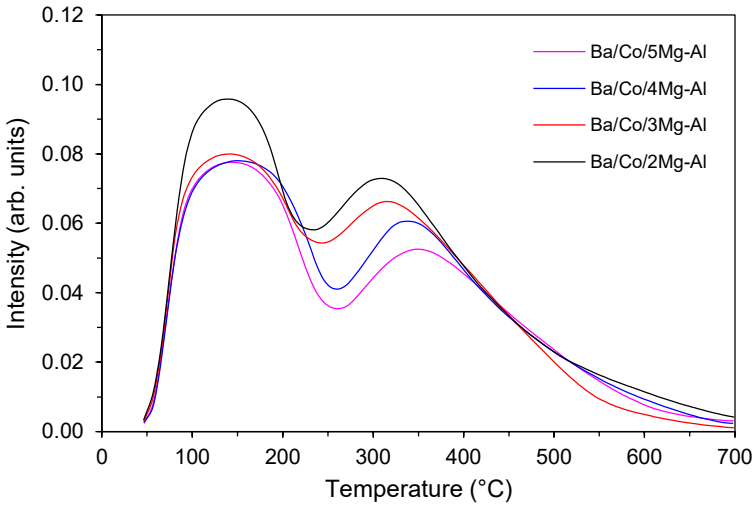

Figure 8. CO_2-TPD profiles of the Ba/Co/Mg-Al catalysts supported on mixed oxides with various Mg/Al molar ratios.

The effect of support composition on the catalyst activity in ammonia synthesis tested at the temperature of 470 °C, under the pressure of 6.3 MPa using a stoichiometric mixture of H_2/N_2, is shown in Table 3. It can be seen that the activity of the Ba/Co/Mg-Al catalysts is similar regardless of the Mg/Al molar ratio in the support. The average reaction rate reaches values of 0.41–0.50 g_{NH_3} g_{cat}^{-1} h^{-1} (for comparison, the activity of the Co/5Mg-Al

without Ba promoter is about five times lower and equals 0.11 g_{NH_3} $g_{cat}{}^{-1}$ h^{-1}). In the literature, the activity of catalysts in ammonia synthesis is generally connected with their basic properties influencing the reaction mechanism [2]. In this respect, the obtained results of catalyst activity are consistent with the results of surface basicity. All the studied catalysts show similar activity, which most likely results from the similar density of basic sites on the catalyst surfaces. Hence, the Mg/Al molar ratio change in the hydrotalcite-derived Mg-Al mixed oxide is therefore of no importance for the final catalytic properties of the obtained Ba/Co/Mg-Al catalysts.

4. Conclusions

In summary, a series of Mg-Al mixed oxides with various Mg/Al molar ratio (from 2 to 5) was prepared using hydrotalcite precursors and used as a support of the barium-promoted cobalt catalyst for ammonia synthesis. The detailed characterization studies and activity measurements in ammonia synthesis reaction allowed us to determine the relationship between the support composition and catalyst properties. The studies revealed that the prepared Mg-Al mixed oxides are good candidates for supports of the cobalt catalysts. However, the support composition does not influence the activity of the Ba/Co/Mg-Al catalysts. The change in Mg/Al molar ratio from 2 to 5 did not significantly influence the properties of the catalysts. All the catalysts are characterized by similar textural, structural, and chemisorption properties. The similar density of basic sites on the surface of studied catalysts was reflected in the comparable performance of these catalysts in the ammonia synthesis reaction.

Author Contributions: Conceptualization, M.Z. and H.R.; Methodology, M.Z., H.R., K.S. and W.R.-P.; Investigation, M.Z., H.R., A.D., K.S., A.O., W.P. and W.R.-P.; Writing—original draft preparation, M.Z. and A.D.; Writing—review and editing, M.Z., H.R. and W.R.-P.; Visualization, H.R. and K.S.; Supervision, M.Z. All authors have read and agreed to the published version of the manuscript.

Funding: This research received no external funding.

Institutional Review Board Statement: Not applicable.

Informed Consent Statement: Not applicable.

Data Availability Statement: All data is available within the paper.

Conflicts of Interest: The authors declare no conflict of interest.

References

1. Smith, C.; Hill, A.K.; Torrente-Murciano, L. Current and future role of Haber–Bosch ammonia in a carbon-free energy landscape. *Energy Environ. Sci.* **2020**, *13*, 331–344. [CrossRef]
2. Humphreys, J.; Lan, R.; Tao, S. Development and recent progress on ammonia synthesis catalysts for Haber–Bosch process. *Adv. Energy Sustain. Res.* **2021**, *2*, 2000043. [CrossRef]
3. Marakatti, V.S.; Gaigneaux, E.M. Recent advances in heterogeneous catalysis for ammonia synthesis. *ChemCatChem* **2020**, *12*, 5838–5857. [CrossRef]
4. Schlögl, R. Catalytic Synthesis of Ammonia—A "Never-Ending Story"? *Angew. Chem. Int. Ed.* **2003**, *42*, 2004–2008. [CrossRef]
5. Hooper, C.W. Ammonia Synthesis: Commercial Practice. In *Catalytic Ammonia Synthesis, Fundamentals and Practice*; Jennings, J.R., Ed.; Springer: New York, NY, USA, 1991; pp. 253–283. [CrossRef]
6. Saito, M.; Itoh, M.; Iwamoto, J.; Li, C.Y.; Machida, K.I. Synergistic Effect of MgO and CeO_2 as a Support for Ruthenium Catalysts in Ammonia Synthesis. *Catal. Lett.* **2006**, *106*, 107–110. [CrossRef]
7. Javaid, R.; Nanba, T. Effect of preparation method and reaction parameters on catalytic activity for ammonia synthesis. *Int. J. Hydrogen Energy* **2021**, *46*, 35209–35218. [CrossRef]
8. Huo, C.; Xia, Q.H.; Pan, M.H.; Liu, H.Z. Efficient La–Ba–MgO Supported Ru Catalysts for Ammonia Synthesis. *Catal. Lett.* **2011**, *141*, 1275. [CrossRef]
9. Yang, X.L.; Zhang, W.Q.; Xia, C.G.; Xiong, X.M.; Mu, X.Y.; Hu, B. Low temperature ruthenium catalyst for ammonia synthesis supported on $BaCeO_3$ nanocrystals. *Catal. Commun.* **2010**, *11*, 867–880. [CrossRef]
10. Wang, Z.; Liu, B.; Lin, J. Highly effective perovskite-type $BaZrO_3$ supported Ru catalyst for ammonia synthesis. *Appl. Catal. A Gen.* **2013**, *458*, 130–136. [CrossRef]

11. Wang, Z.; Ma, Y.; Lin, J. Ruthenium catalyst supported on high-surface-area basic ZrO_2 for ammonia synthesis. *J. Mol. Catal. A Chem.* **2013**, *378*, 307–313. [CrossRef]
12. Lin, B.; Wu, Y.; Fang, B.; Li, C.; Ni, J.; Wang, X.; Lin, J.; Jiang, L. Ru surface density effect on ammonia synthesis activity and hydrogen poisoning of ceria-supported Ru catalysts. *Chin. J. Catal.* **2021**, *42*, 1712–1723. [CrossRef]
13. Ma, Z.; Zhao, S.; Pei, X.; Xiong, X.; Hu, B. New insights into the support morphology-dependent ammonia synthesis activity of Ru/CeO_2 catalysts. *Catal. Sci. Technol.* **2017**, *7*, 191–199. [CrossRef]
14. Imamura, K.; Miyahara, S.; Kawano, Y.; Sato, K.; Nakasaka, Y.; Nagaoka, K. Kinetics of ammonia synthesis over Ru/Pr_2O_3. *J. Taiwan Inst. Chem. Eng.* **2019**, *105*, 50–56. [CrossRef]
15. Zhang, L.; Lin, J.; Ni, J.; Wang, R.; Wei, K. Highly efficient Ru/Sm_2O_3-CeO_2 catalyst for ammonia synthesis. *Catal. Commun.* **2011**, *15*, 23–26. [CrossRef]
16. Miyahara, S.; Sato, K.; Kawano, Y.; Imamura, K.; Ogura, Y.; Tsujimaru, K.; Nagaoka, K. Ammonia synthesis over lanthanoid oxide–supported ruthenium catalysts. *Catal. Today* **2021**, *376*, 36–40. [CrossRef]
17. Sato, K.; Imamura, K.; Kawano, Y.; Miyahara, S.; Yamamoto, Y.; Matsumura, S.; Nagaoka, K. A low-crystalline ruthenium nano-layer supported on praseodymium oxide as an active catalyst for ammonia synthesis. *Chem. Sci.* **2017**, *8*, 674–679. [CrossRef]
18. Hagen, S.; Barfod, R.; Fehrmann, R.; Jacobsen, C.J.H.; Teunissen, H.T.; Chorkendorff, I. Ammonia synthesis with barium-promoted iron–cobalt alloys supported on carbon. *J. Catal.* **2003**, *214*, 327–335. [CrossRef]
19. Hagen, S.; Barfod, R.; Fehrmann, R.; Jacobsen, C.J.H.; Teunissen, H.T.; Ståhl, K.; Chorkendorff, I. New efficient catalyst for ammonia synthesis: Barium-promoted cobalt on carbon. *Chem. Commun.* **2002**, *11*, 1206–1207. [CrossRef]
20. Raróg-Pilecka, W.; Karolewska, M.; Truszkiewicz, E.; Iwanek, E.; Mierzwa, B. Cobalt catalyst doped with cerium and barium obtained by co-precipitation method for ammonia synthesis process. *Catal. Lett.* **2011**, *141*, 678–684. [CrossRef]
21. Tarka, A.; Patkowski, W.; Zybert, M.; Ronduda, H.; Wieciński, P.; Adamski, P.; Sarnecki, A.; Moszyński, D.; Raróg-Pilecka, W. Synergistic interaction of cerium and barium-New insight into the promotion effect in cobalt systems for ammonia synthesis. *Catalysts* **2020**, *10*, 658. [CrossRef]
22. Zybert, M.; Wyszyńska, M.; Tarka, A.; Patkowski, W.; Ronduda, H.; Mierzwa, B.; Kępiński, L.; Sarnecki, A.; Moszyński, D.; Raróg-Pilecka, W. Surface enrichment phenomenon in the Ba-doped cobalt catalyst for ammonia synthesis. *Vacuum* **2019**, *168*, 108831. [CrossRef]
23. Karolewska, M.; Truszkiewicz, E.; Mierzwa, B.; Kępiński, L.; Raróg-Pilecka, W. Ammonia synthesis over cobalt catalysts doped with cerium and barium. Effect of the ceria loading. *Appl. Catal. A* **2012**, *445–446*, 280–286. [CrossRef]
24. Zybert, M.; Tarka, A.; Mierzwa, B.; Kępiński, L.; Raróg-Pilecka, W. Promotion effect of lanthanum on the Co/La/Ba ammonia synthesis catalysts—the influence of lanthanum content. *Appl. Catal. A* **2016**, *515*, 16–24. [CrossRef]
25. Raróg-Pilecka, W.; Miśkiewicz, E.; Kępiński, L.; Kaszkur, Z.; Kielar, K.; Kowalczyk, Z. Ammonia synthesis over barium-promoted cobalt catalysts supported on graphitised carbon. *J. Catal.* **2007**, *249*, 24–33. [CrossRef]
26. Karolewska, M.; Truszkiewicz, E.; Wściseł, M.; Mierzwa, B.; Kępiński, L.; Raróg-Pilecka, W. Ammonia synthesis over a Ba and Ce-promoted carbon-supported cobalt catalyst. Effect of the cerium addition and preparation procedure. *J. Catal.* **2013**, *303*, 130–134. [CrossRef]
27. Lin, B.; Qi, Y.; Wei, K.; Lin, J. Effect of pretreatment on ceria-supported cobalt catalyst for ammonia synthesis. *RSC Adv.* **2014**, *4*, 38093–38102. [CrossRef]
28. Lin, B.; Liu, Y.; Heng, L.; Ni, J.; Lin, J.; Jiang, L. Effect of ceria morphology on the catalytic activity of Co/CeO_2 catalyst for ammonia synthesis. *Catal. Commun.* **2017**, *101*, 15–19. [CrossRef]
29. Lin, B.; Liu, Y.; Heng, L.; Ni, J.; Lin, J.; Jiang, L. Effect of barium and potassium promoter on Co/CeO_2 catalysts in ammonia synthesis. *J. Rare Earths* **2018**, *36*, 703–707. [CrossRef]
30. Sato, K.; Miyahara, S.; Tsujimaru, K.; Wada, Y.; Toriyama, T.; Yamamoto, T.; Matsumura, S.; Inazu, K.; Mohri, H.; Iwasa, T.; et al. Barium oxide encapsulating cobalt nanoparticles supported on magnesium oxide: Active non-noble metal catalysts for ammonia synthesis under mild reaction conditions. *ACS Catal.* **2021**, *11*, 13050–13061. [CrossRef]
31. Ronduda, H.; Zybert, M.; Patkowski, W.; Tarka, A.; Jodłowski, P.; Kępiński, L.; Sarnecki, A.; Moszyński, D.; Raróg-Pilecka, W. Tuning the catalytic performance of Co/Mg-La system for Ammonia synthesis via the active phase precursor introduction method. *Appl. Catal. A* **2020**, *598*, 117553. [CrossRef]
32. Ronduda, H.; Zybert, M.; Patkowski, W.; Tarka, A.; Ostrowski, A.; Raróg-Pilecka, W. Kinetic studies of ammonia synthesis over a barium-promoted cobalt catalyst supported on magnesium–lanthanum mixed oxide. *J. Taiwan Inst. Chem. Eng.* **2020**, *114*, 241–248. [CrossRef]
33. Ronduda, H.; Zybert, M.; Patkowski, W.; Ostrowski, A.; Jodłowski, P.; Szymański, D.; Kępiński, L.; Raróg-Pilecka, W. Boosting the catalytic performance of Co/Mg/La catalyst for ammonia synthesis by selecting a pre-treatment method. *Catalysts* **2021**, *11*, 941. [CrossRef]
34. Ronduda, H.; Zybert, M.; Patkowski, W.; Ostrowski, A.; Jodłowski, P.; Szymański, D.; Kępiński, L.; Raróg-Pilecka, W. A high performance barium-promoted cobalt catalyst supported on magnesium–lanthanum mixed oxide for ammonia synthesis. *RSC Adv.* **2021**, *11*, 14218–14228. [CrossRef] [PubMed]
35. Ronduda, H.; Zybert, M.; Patkowski, W.; Ostrowski, A.; Jodłowski, P.; Szymański, D.; Kępiński, L.; Raróg-Pilecka, W. Development of cobalt catalyst supported on $MgO–Ln_2O_3$ (Ln = La, Nd, Eu) mixed oxide systems for ammonia synthesis. *Int. J. Hydrogen Energy* **2022**, *47*, 6666–6678. [CrossRef]

36. Wu, J.; Li, J.; Gong, Y.; Kitano, M.; Inoshita, T.; Hosono, H. Intermetallic Electride Catalyst as a Platform for Ammonia Synthesis. *Angew. Chem. Int. Ed.* **2019**, *58*, 825–829. [CrossRef]
37. Inoue, Y.; Kitano, M.; Tokunari, M.; Taniguchi, T.; Ooya, K.; Abe, H.; Niwa, Y.; Sasase, M.; Hara, M.; Hosono, H. Direct Activation of Cobalt Catalyst by $12CaO{\cdot}7Al_2O_3$ Electride for Ammonia Synthesis. *ACS Catal.* **2019**, *9*, 1670–1679. [CrossRef]
38. Gao, W.; Wang, P.; Guo, J.; Chang, F.; He, T.; Wang, Q.; Wu, G.; Chen, P. Barium Hydride-Mediated Nitrogen Transfer and Hydrogenation for Ammonia Synthesis: A Case Study of Cobalt. *ACS Catal.* **2017**, *7*, 3654–3661. [CrossRef]
39. Wang, P.; Chang, F.; Gao, W.; Guo, J.; Wu, G.; He, T.; Chen, P. Breaking scaling relations to achieve low-temperature ammonia synthesis through LiH-mediated nitrogen transfer and hydrogenation. *Nat. Chem.* **2017**, *9*, 64–70. [CrossRef]
40. Ye, T.-N.; Park, S.-W.; Lu, Y.; Li, J.; Wu, J.; Sasase, M.; Kitano, M.; Hosono, H. Dissociative and Associative Concerted Mechanism for Ammonia Synthesis over Co-Based Catalyst. *J. Am. Chem. Soc.* **2021**, *143*, 12857–12866. [CrossRef]
41. Cavani, F.; Trifiro, F.; Vaccari, A. Hydrotalcite-type anionic clays: Preparation, properties and applications. *Catal. Today* **1991**, *11*, 173–301. [CrossRef]
42. Di Cosimo, J.I.; Díez, V.K.; Xu, M.; Iglesia, E.; Apesteguía, C.R. Structure and surface and catalytic properties of Mg-Al basic oxides. *J. Catal.* **1998**, *178*, 499–510. [CrossRef]
43. Fan, G.; Li, F.; Evans, D.G.; Duan, X. Catalytic applications of layered double hydroxides: Recent advances and perspectives. *Chem. Soc. Rev.* **2014**, *43*, 7040–7066. [CrossRef] [PubMed]
44. Xu, M.; Wei, M. Layered double hydroxide-based catalysts: Recent advances in preparation, structure, and applications. *Adv. Funct. Mater.* **2018**, *28*, 1802943. [CrossRef]
45. Hájek, M.; Kutálek, P.; Smoláková, L.; Troppová, I.; Čapek, L.; Kubička, D.; Kocík, J.; Thanh, D.N. Transesterification of rapeseed oil by Mg–Al mixed oxides with various Mg/Al molar ratio. *Chem. Eng. J.* **2015**, *263*, 160–167. [CrossRef]
46. Ni, J.; Jing, B.; Lin, J.; Lin, B.; Zhao, Z.; Jiang, L. Effect of rare earth on the performance of Ru/MgAl-LDO catalysts for ammonia synthesis. *J. Rare Earths* **2018**, *36*, 135–141. [CrossRef]
47. Seetharamulu, P.; Siva Kumar, V.; Padmasri, A.H.; David Raju, B.; Rama Rao, K.S. A highly active nano-Ru catalyst supported on novel Mg–Al hydrotalcite precursor for the synthesis of ammonia. *J. Mol. Catal. A Chem.* **2007**, *263*, 253–258. [CrossRef]
48. Palmer, S.J.; Spratt, H.J.; Frost, R.L. Thermal decomposition of hydrotalcites with variable cationic ratios. *J. Therm. Anal. Calorim.* **2009**, *95*, 123–129. [CrossRef]
49. Roelofs, J.C.A.A.; van Bokhoven, J.A.; Jos van Dillen, A.; Geus, J.W.; de Jong, K.P. The thermal decomposition of Mg–Al hydrotalcites: Effects of interlayer anions and characteristics of the final structure. *Chem. Eur. J.* **2002**, *8*, 5571–5579. [CrossRef]
50. Sing, K.S.W. Reporting physisorption data for gas/solid systems with special reference to the determination of surface area and porosity (Recommendations 1984). *Pure Appl. Chem.* **1985**, *57*, 603–619. [CrossRef]
51. Jinesh, C.M.; Antonyraj, C.A.; Kannan, S. Allylbenzene isomerisation over as-synthesised MgAl and NiAl containing LDHs: Basicity-activity relationships. *Appl. Clay Sci.* **2010**, *48*, 243–249. [CrossRef]
52. Veloso, C.O.; Perez, C.N.; de Souza, B.M.; Lima, E.C.; Dias, A.G.; Monteiro, J.L.F.; Henriques, C.A. Condensation of glyceraldehyde over Mg–Al-mixed oxides derived from hydrotalcites. *Microporous Mesoporous Mater.* **2008**, *107*, 23–30. [CrossRef]
53. Fishel, C.T.; Davis, R.J. Characterisation of Mg–Al mixed oxides by temperature-programmed reaction of 2-propanol. *Langmuir* **1994**, *10*, 159–165. [CrossRef]
54. Kuśtrowski, P.; Chmielarz, L.; Bożek, E.; Sawalha, M.; Roessner, F. Acidity and basicity of hydrotalcite derived mixed Mg–Al oxides studied by test reaction of MBOH conversion and temperature programmed desorption of NH_3 and CO_2. *Mater. Res. Bull.* **2004**, *39*, 263–281. [CrossRef]
55. Kuśtrowski, P.; Sułkowska, D.; Chmielarz, L.; Rafalska-Łasocha, A.; Dudek, B.; Dziembaj, R. Influence of thermal treatment conditions on the activity of hydrotalcite-derived Mg–Al oxides in the aldol condensation of acetone. *Microporous Mesoporous Mater.* **2005**, *78*, 11–22. [CrossRef]